



OPEN

## Profiles of movement speed and positional variability based on extended LQG for various noises

Yoshiaki Taniai

Stochastic optimal control has been studied to explain the characteristics of human upper-arm reaching movements. The optimal movement based on an extended linear quadratic Gaussian (LQG) demonstrated that control-dependent noise is the essential factor of the speed-accuracy trade-off in the point-to-point reaching movement. Furthermore, the extended LQG reproduced the profiles of movement speed and positional variability. However, the expected value and variance were computed based on the Monte Carlo method in these studies, which is not considered efficient. In this study, I obtained update equations to efficiently compute the expected value and variance based on the extended LQG. Using the update equations, I computed the profiles of simulated movement speed and positional variability for various amplitudes of noises in a point-to-point reaching movement. The profiles of movement speed were basically bell-shaped for the noises. The speed peak was changed by the control-dependent noise and state-dependent observation noise. The positional variability changed for various noises, and the period during which the variability changed differed with the noise type. Efficient computation in stochastic optimal control based on the extended LQG would contribute to the elucidation of motor control under various noises.

Upper-arm reaching movement is one of the most common movements studied for examining motor control. Stochastic optimal control has been studied to explain the characteristics of human upper-arm reaching movement. The studies of stochastic optimal control are based on the assumption that the reaching movement is determined to optimize an evaluation function in the presence of conceivable noise that affects the neurophysiological processing of the living body. In the reaching movement, the speed profile of the hand is bell-shaped<sup>1</sup>, and the positional variability has the highest value around the middle of the movement, decreasing thereafter<sup>2-5</sup>. In addition, the trade-off between speed and accuracy of the movement is well known<sup>6</sup>.

Harris and Wolpert proposed the minimum variance model<sup>7</sup>. The noise considered in the minimum variance model is signal-dependent noise that depends on the magnitude of the signal and is also known as multiplicative noise. The signal-dependent noise increases with the amplitude of the control signal and is called control-dependent noise. The minimum variance model is the minimization of total positional variance in the post-movement duration. The trajectory based on the minimum variance model reproduces the trajectory and speed profile of human upper-arm reaching movement. Todorov proposed the extended linear quadratic Gaussian (LQG) framework to examine stochastic optimal control and sensorimotor estimation. The extended LQG is a framework that can efficiently solve optimal feedback control under biologically conceivable noise, which is not only signal-dependent noise but also signal-independent noise, state-dependent noise, and state-independent noise<sup>8</sup>. The signal-independent noise is the noise that does not depend on the magnitude of the signal and is also called additive noise. In the framework, the movement dynamic system consists of state noise, which is the state-independent noise that does not depend on the magnitude of the state, as well as control-dependent noise. The feedback system consists of the state-dependent and state-independent observation noise, and the state estimation system consists of the state-independent noise, called internal estimation noise (for more details of noises, refer to “Framework of extended LQG” in the section “Methods”). The optimal movement based on the extended LQG demonstrated that control-dependent noise is the essential factor of the speed-accuracy trade-off and that the optimal speed profile is bell-shaped. In addition, the extended LQG can reproduce the profile of positional variability<sup>5,9</sup>. Furthermore, aspect ratio, surface area, and orientation of variability ellipses in the movement end vary with the direction under state-dependent observation noise<sup>9</sup>, and these characteristics have been reported in human movements<sup>10</sup>. On the other hand, a novel motor learning paradigm that varies the state-dependent observation noise of visual feedback in the limbs was developed to test the optimal hybrid feedforward

Graduate School of Engineering, University of Fukui, 3-9-1 Bunkyo, Fukui 910-8507, Japan. email: [taniai@u-fukui.ac.jp](mailto:taniai@u-fukui.ac.jp)

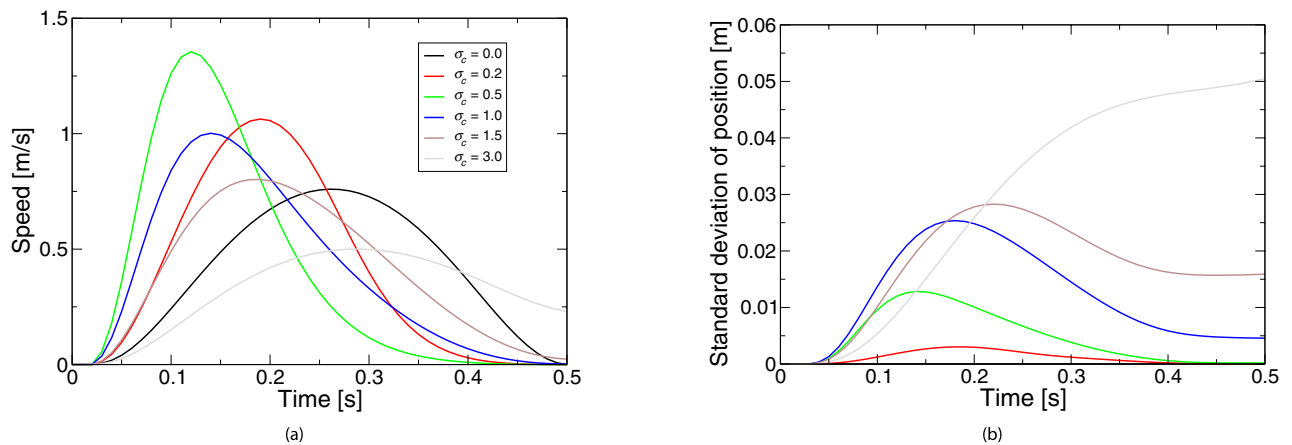


**Figure 1.** Simulated movements based on the extended LQG for the coefficient  $\sigma_c$  of control-dependent noise: (a) speed, (b) positional variability. The legend of the subfigure (b) is the same as the subfigure (a).

and feedback controller based on the extended LQG<sup>11</sup>. The controller reproduced the human-adapted complex reaching trajectory. However, in the studies mentioned above about the extended LQG, the expected value and variance were computed based on the Monte Carlo method. The Monte Carlo method computes the expected value by repeating many trials and requires much computation time. It is important to efficiently obtain the expected value and variance to investigate whether the optimal feedback control can reproduce the characteristics of human movement in environments related to the effects of various noises.

In this study, I obtained update equations to efficiently compute the expected value and variance based on the extended LQG. Using the update equations, I computed the profiles of simulated movement speed and positional variability for various amplitudes of noises in a point-to-point reaching movement. In the computations of simulated movements, control-dependent noise is always considered, while the other noise is considered from the state-dependent observation noise, state noise, state-independent observation noise, and internal estimation noise.

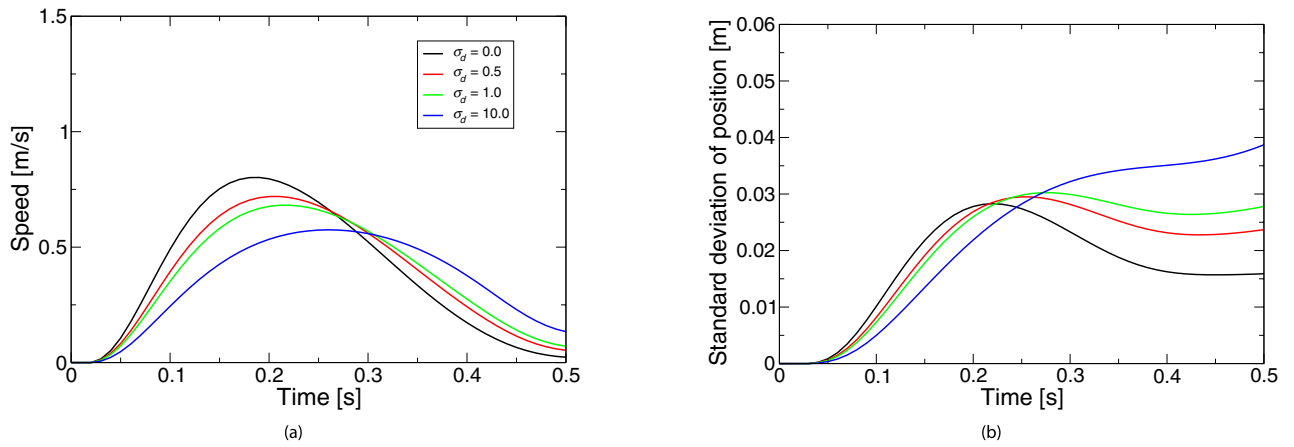
## Results

Figure 1 represents the simulated movements based on the extended LQG for the coefficient  $\sigma_c$  of the control-dependent noise. Figure 1a shows the speed profiles. The profiles were almost bell-shaped. The speed peak was about half the movement duration when the noise was absent (i.e.,  $\sigma_c = 0$ ). Although the peak appeared earlier when the noise was slight ( $\sigma_c = 0.2, 0.5$ ), and when the noise was larger ( $\sigma_c = 1.0, 1.5, 3.0$ ), the peak appeared later. When the noise was further larger ( $\sigma_c = 3.0$ ), the velocity at the movement's end was far from zero. Figure 1b shows the profiles of positional variability. When the noise was absent ( $\sigma_c = 0$ ), the standard deviation of the position was zero (i.e., the line was identical with the X-axis). When the noise was larger, the variability peak appeared later and the positional variability was larger over the movement. When the noise was even larger ( $\sigma_c = 3.0$ ), the peak disappeared (i.e., the variability increased monotonically). The optimal movement when  $\sigma_c$  was 1.5 was the result for the basic parameter set. In the basic parameters, only the control-dependent noise was considered. The profiles of movement speed and positional variability resembled the characteristics reported by past studies<sup>2-4</sup>.

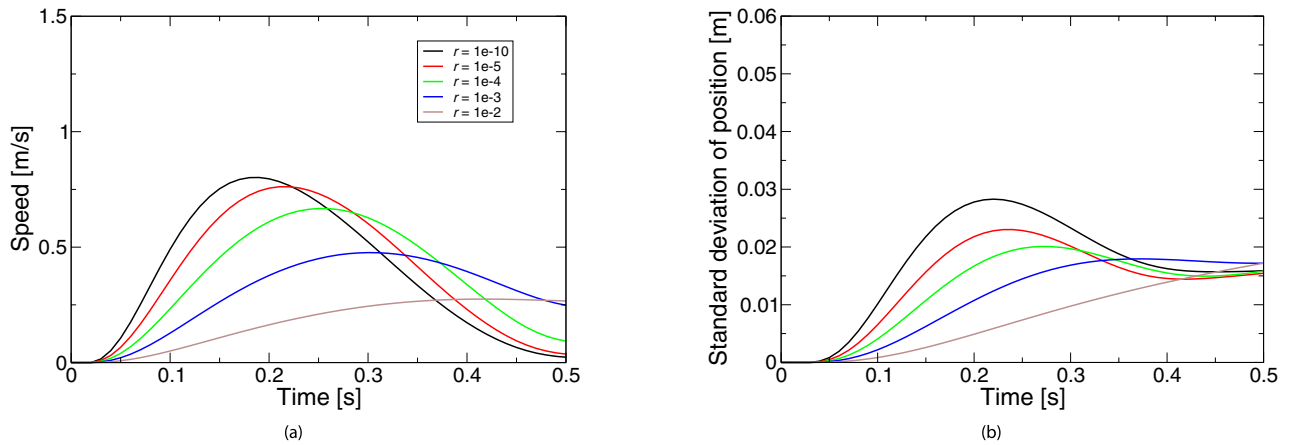
Figure 2 represents the simulated movements based on the extended LQG for the coefficient  $\sigma_d$  of the state-dependent observation noise. Figure 2a shows the speed profiles. All profiles were almost bell-shaped. As the noise became larger, the speed peak appeared later. Figure 2b shows the profiles of positional variability. Unlike the case of control-dependent noise, no significant change occurred up to about half of the movement, although the variability was larger in the latter half of the movement.

Figure 3 represents the simulated movements based on the extended LQG for the coefficient  $r$  of the control cost. Figure 3a shows the speed profiles. As the control cost was larger, the speed peak appeared later. Figure 3b shows the profiles of positional variability. Unlike the case of state-dependent observation noise, there was a large change up to about half of the movement but little change after half the movement. In other words, as the ratio of state cost increased, the variability around the middle of the movement became larger.

Figure 4 represents the simulated movements based on the extended LQG for the coefficient  $\sigma_\xi$  of the state noise. Figure 4a shows the speed profiles. The profiles were mostly bell-shaped and largely remained unchanged by the state noise. This characteristic was also confirmed for state-independent observation noise (Fig. 5a) and internal estimation noise (Fig. 6a). The scaling factor of the state-dependent observation noise in these results was zero ( $\sigma_d = 0$ ). Although the resulting graph is not shown, the velocity peak appears slightly later when the scaling factor is not zero. Figure 4b shows the positional variability. As the state noise became larger, the variability increased over the movement. On the other hand, the variability in the state-independent observation noise and internal estimation noise did not change almost from the beginning to the middle of the movement (Figs. 5b, 6b).



**Figure 2.** Simulated movements based on the extended LQG for the coefficient  $\sigma_d$  of state-dependent observation noise: (a) speed, (b) positional variability. The legend of the subfigure (b) is the same as the subfigure (a).



**Figure 3.** Simulated movements based on the extended LQG for the coefficient  $r$  of control cost: (a) speed, (b) positional variability. The legend of the subfigure (b) is the same as the subfigure (a).

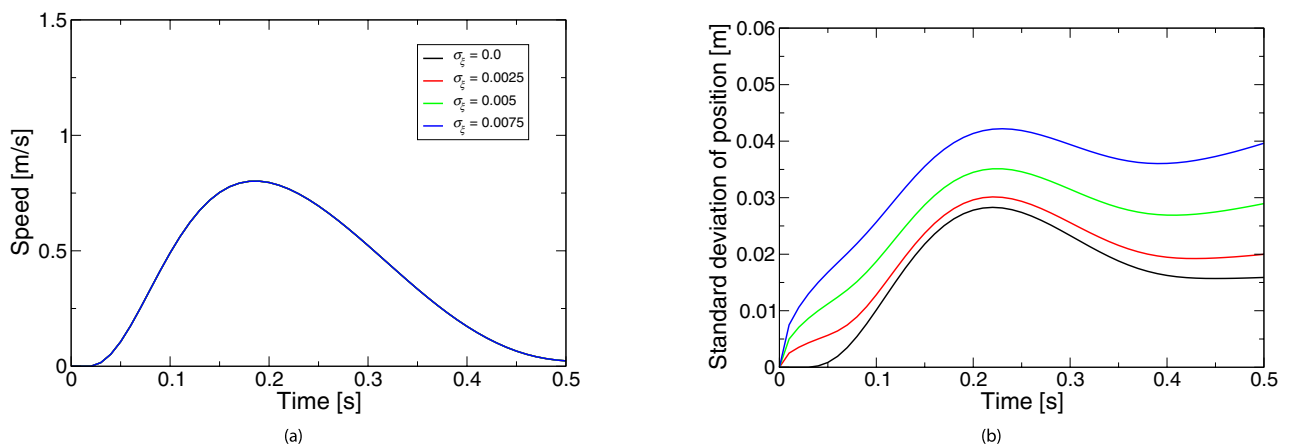


**Figure 4.** Simulated movements based on the extended LQG for the coefficient  $\sigma_z$  of state noise: (a) speed, (b) positional variability. The legend of the subfigure (b) is the same as the subfigure (a).

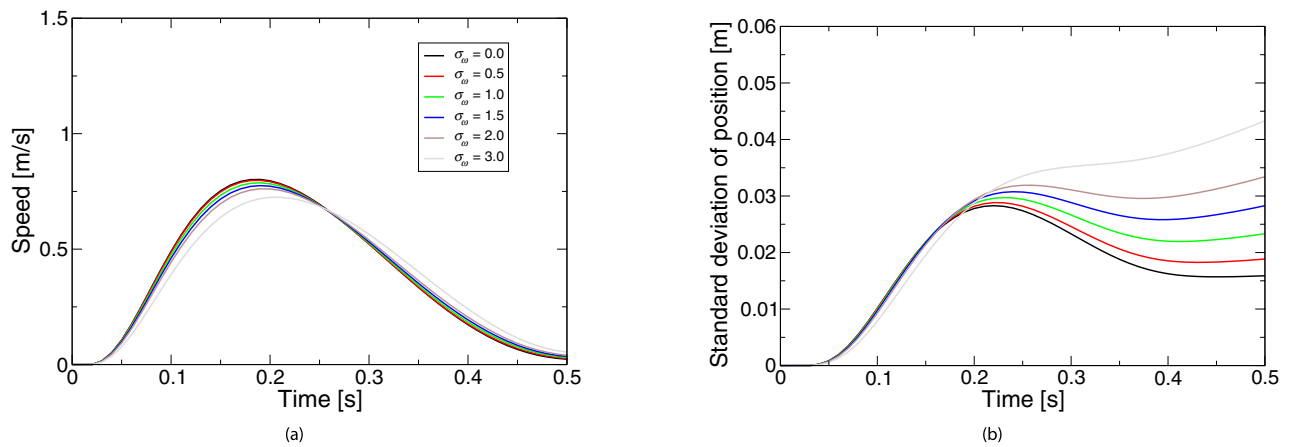


**Figure 5.** Simulated movements based on the extended LQG for the coefficient  $\sigma_{\omega}$  of state-independent observation noise: **(a)** speed, **(b)** positional variability. The legend of the subfigure **(b)** is the same as the subfigure **(a)**.

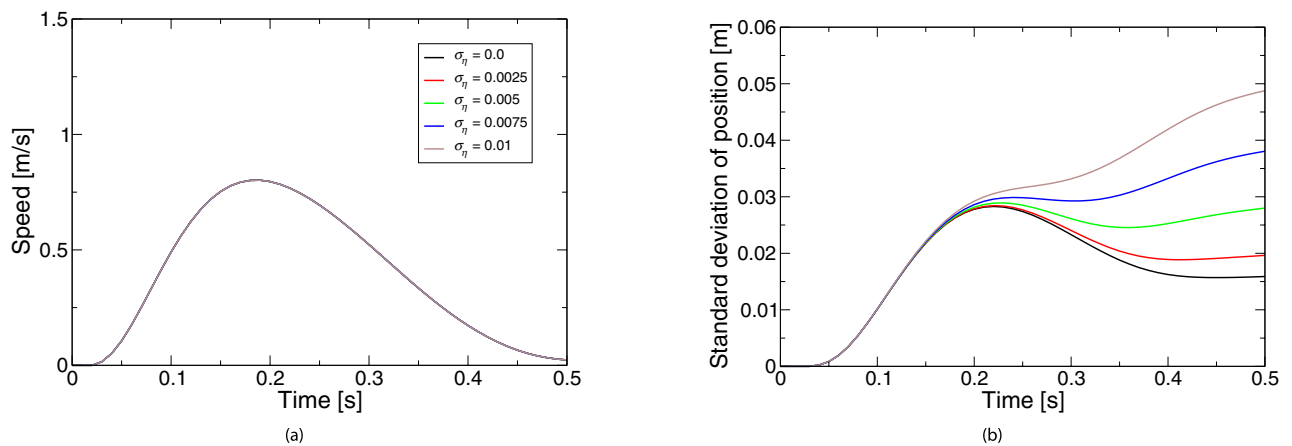


**Figure 6.** Simulated movements based on the extended LQG for the coefficient  $\sigma_{\eta}$  of internal estimation noise: **(a)** speed, **(b)** positional variability. The legend of the subfigure **(b)** is the same as the subfigure **(a)**.

## Discussion

I obtained update equations to efficiently compute the expected value and variance based on the extended LQG. Using the update equations, I computed the profiles of simulated movement speed and positional variability for various amplitudes of noises in a point-to-point reaching movement. The speed peak was changed by the control-dependent noise and state-dependent observation noise. The positional variability changes for various noises, and the period during which the variability changed differed with the noise type. The results show that multiplicative noise is an important factor in characterizing the profiles of positional variability and movement speed and that additive noise is an important factor in characterizing the profiles of positional variability. These characteristics would be helpful in how motor control based on extended LQG appears in the presence of various disturbances.

Stochastic optimal control has been studied to explain the characteristics of human upper-arm reaching movement. In particular, the extended LQG framework has been verified for movement tasks, including various disturbances<sup>5,8,9,11</sup>. The disturbances can be treated as noise in the extended LQG. However, in the previous studies, the expected value and variance of the optimal movement were computed based on the Monte Carlo method. The Monte Carlo method computes the expected value by repeating many trials and requires much computation time. In this study, the updated equations provided an efficient computation of expected value and variance. Efficient computation in stochastic optimal control based on the extended LQG would contribute to the elucidation of motor control under various disturbances.

## Methods

I computed the movement speed and positional variability based on the extended LQG<sup>8</sup> for various amplitudes of noises. Instead of using Monte Carlo method, I obtained update equations to compute the mean and variance of state variables.

**Framework of extended LQG.** The linear movement dynamic system in discrete time  $t$  is given as:

$$\mathbf{x}_{t+1} = A\mathbf{x}_t + B\mathbf{u}_t + \boldsymbol{\xi}_t + \sum_{i=1}^c \epsilon_t^i C_i \mathbf{u}_t \tag{1}$$

where  $A$  and  $B$  are the dynamic system matrices,  $\mathbf{x}$  is the state variables, and  $\mathbf{u}$  is the control signal. State noise  $\boldsymbol{\xi}$  is state-independent noise which is Gaussian with mean 0 and covariance  $\Omega^\xi \geq 0$ . The noise  $\epsilon$  related to control-dependent noise is Gaussian with mean 0 and covariance  $\Omega^\epsilon = \mathbf{I}$ .  $C$  is the scaling matrix for control-dependent noise. The matrix  $C$  is  $BF$ , where  $F$  is the scaling factor. It is already known that the initial state is mean  $\hat{\mathbf{x}}_1$  and covariance  $\Sigma_1$ .

The feedback system is as given below:

$$\mathbf{y}_t = H\mathbf{x}_t + \boldsymbol{\omega}_t + \sum_{i=1}^d \epsilon_t^i D_i \mathbf{x}_t \tag{2}$$

where  $\mathbf{y}$  is the feedback signal and  $H$  is the observation matrix. State-independent observation noise  $\boldsymbol{\omega}$  is Gaussian with mean 0 and covariance  $\Omega^\omega \geq 0$ . The noise  $\epsilon$  related to state-dependent observation noise is Gaussian with mean 0 and covariance  $\Omega^\epsilon = \mathbf{I}$ .  $D$  is the scaling matrix for state-dependent observation noise.

The state estimate  $\hat{\mathbf{x}}$  is calculated as given below:

$$\hat{\mathbf{x}}_{t+1} = A\hat{\mathbf{x}}_t + B\mathbf{u}_t + K_t(\mathbf{y}_t - H\hat{\mathbf{x}}_t) + \boldsymbol{\eta}_t \tag{3}$$

where  $K$  is the filter gain matrix and internal estimation noise  $\boldsymbol{\eta}$  is Gaussian noise with mean 0 and covariance  $\Omega^\eta \geq 0$ .

Cost per step is calculated as given below:

$$\mathbf{x}_t^T Q_t \mathbf{x}_t + \mathbf{u}_t^T R \mathbf{u}_t \tag{4}$$

where  $Q$  is the matrix of the state cost and  $R$  is the matrix of the control cost.

The optimal control  $\mathbf{u}$  is recursively computed in the opposite direction over a period of time, as follows:

$$\mathbf{u}_t = -L_t \hat{\mathbf{x}}_t \tag{5}$$

$$\begin{aligned} L_t &= \left\{ R + B^T S_{t+1}^x B + \sum_i C_i^T (S_{t+1}^x + S_{t+1}^\epsilon) C_i \right\}^{-1} B^T S_{t+1}^x A \\ S_t^x &= Q_t + A^T S_{t+1}^x (A - BL_t) + \sum_i D_i^T K_t^T S_{t+1}^\epsilon K_t D_i \\ S_t^\epsilon &= A^T S_{t+1}^x BL_t + (A - K_t H)^T S_{t+1}^\epsilon (A - K_t H) \\ s_t &= \text{tr} \left\{ S_{t+1}^x \Omega^\xi + S_{t+1}^\epsilon (\Omega^\xi + \Omega^\eta + K_t \Omega^\omega K_t^T) \right\} + s_{t+1} \end{aligned} \tag{6}$$

where  $L$  is the control gain matrix. It is initialized as follows:  $S_n^x = Q_n$ ,  $S_n^\epsilon = 0$ , and  $s_n = 0$ . Total expected cost is calculated as follows:

$$\hat{\mathbf{x}}_1^T S_1^x \hat{\mathbf{x}}_1 + \text{tr} \{ (S_1^x + S_1^\epsilon) \Sigma_1 \} + s_1. \tag{7}$$

The optimal filter is recursively computed forward in time as follows:

$$\hat{\mathbf{x}}_{t+1} = (A - BL_t) \hat{\mathbf{x}}_t + K_t(\mathbf{y}_t - H\hat{\mathbf{x}}_t) + \boldsymbol{\eta}_t \tag{8}$$

$$\begin{aligned} K_t &= A \Sigma_t^\epsilon H^T \left\{ H \Sigma_t^\epsilon H^T + \Omega^\omega + \sum_i D_i (\Sigma_t^\epsilon + \Sigma_t^{\hat{\mathbf{x}}} + \Sigma_t^{\hat{\mathbf{e}}} + \Sigma_t^{\hat{\mathbf{x}}}) D_i^T \right\}^{-1} \\ \Sigma_{t+1}^\epsilon &= \Omega^\xi + \Omega^\eta + (A - K_t H) \Sigma_t^\epsilon A^T + \sum_i C_i L_t \Sigma_t^{\hat{\mathbf{x}}} L_t^T C_i^T \\ \Sigma_{t+1}^{\hat{\mathbf{x}}} &= \Omega^\eta + K_t H \Sigma_t^\epsilon A^T + (A - BL_t) \Sigma_t^{\hat{\mathbf{x}}} (A - BL_t)^T \\ &\quad + (A - BL_t) \Sigma_t^{\hat{\mathbf{e}}} H^T K_t^T + K_t H \Sigma_t^\epsilon \hat{\mathbf{x}} (A - BL_t)^T \\ \Sigma_{t+1}^{\hat{\mathbf{e}}} &= (A - BL_t) \Sigma_t^{\hat{\mathbf{e}}} (A - K_t H)^T - \Omega^\eta. \end{aligned} \tag{9}$$

It is initialized as follows:  $\Sigma_1^\epsilon = \Sigma_1$ ,  $\Sigma_1^{\hat{\mathbf{x}}} = \hat{\mathbf{x}}_1 \hat{\mathbf{x}}_1^T$ , and  $\Sigma_1^{\hat{\mathbf{e}}} = 0$ .

**Mean and variance of state variables.** The update equations used to compute the mean and variance of state variables were obtained from Eq. (1) and the following equations.

$$\hat{\mathbf{x}}_{t+1} = (A - BL_t) \hat{\mathbf{x}}_t + K_t H \mathbf{e}_t + K_t \boldsymbol{\omega}_t + \boldsymbol{\eta}_t + \sum_i \epsilon_t^i K_t D_i (\mathbf{e}_t + \hat{\mathbf{x}}_t) \tag{10}$$

$$\mathbf{e}_{t+1} = (A - K_t H) \mathbf{e}_t + \boldsymbol{\xi}_t - K_t \boldsymbol{\omega}_t - \boldsymbol{\eta}_t - \sum_i \varepsilon_t^i C_i L_t \hat{\mathbf{x}}_t - \sum_i \varepsilon_t^i K_t D_i (\mathbf{e}_t + \hat{\mathbf{x}}_t) \quad (11)$$

where the estimation error  $\mathbf{e}_t$  is  $\mathbf{x}_t - \hat{\mathbf{x}}_t$ . Equations (10) and (11) are derived from Eqs. (2) and (3), and Eqs. (1) and (10), respectively.

The mean of state variables can be computed sequentially by applying the following update equations.

$$E[\mathbf{x}_{t+1}] = A E[\mathbf{x}_t] - B L_t E[\hat{\mathbf{x}}_t] \quad (12)$$

$$E[\hat{\mathbf{x}}_{t+1}] = (A - B L_t) E[\hat{\mathbf{x}}_t] + K_t H E[\mathbf{e}_t] \quad (13)$$

$$E[\mathbf{e}_{t+1}] = (A - K_t H) E[\mathbf{e}_t] \quad (14)$$

The variance of state variables can be computed sequentially by using the following update equations:

$$\begin{aligned} \text{var}[\mathbf{x}_{t+1}] = & A \text{var}[\mathbf{x}_t] A^\top \\ & - A \text{cov}[\mathbf{x}_t, \hat{\mathbf{x}}_t] L_t^\top B^\top \\ & - B L_t \text{cov}[\hat{\mathbf{x}}_t, \mathbf{x}_t] A^\top \\ & + B L_t \text{var}[\hat{\mathbf{x}}_t] L_t^\top B^\top \\ & + \Omega^\xi + \sum_i C_i L_t \Sigma_t^{\hat{\mathbf{x}}} L_t^\top C_i^\top \end{aligned} \quad (15)$$

$$\begin{aligned} \text{cov}[\mathbf{x}_{t+1}, \hat{\mathbf{x}}_{t+1}] = & A \text{cov}[\mathbf{x}_t, \hat{\mathbf{x}}_t] (A - B L_t)^\top \\ & + A \text{cov}[\mathbf{x}_t, \mathbf{e}_t] H^\top K_t^\top \\ & - B L_t \text{var}[\hat{\mathbf{x}}_t] (A - B L_t)^\top \\ & - B L_t \text{cov}[\hat{\mathbf{x}}_t, \mathbf{e}_t] H^\top K_t^\top \end{aligned} \quad (16)$$

$$\begin{aligned} \text{var}[\hat{\mathbf{x}}_{t+1}] = & (A - B L_t) \text{var}[\hat{\mathbf{x}}_t] (A - B L_t)^\top \\ & + (A - B L_t) \text{cov}[\hat{\mathbf{x}}_t, \mathbf{e}_t] H^\top K_t^\top \\ & + K_t H \text{cov}[\mathbf{e}_t, \hat{\mathbf{x}}_t] (A - B L_t)^\top \\ & + K_t H \text{var}[\mathbf{e}_t] H^\top K_t^\top \\ & + K_t \Omega^\omega K_t^\top + \Omega^\eta \\ & + \sum_i K_t D_i \Sigma_t^{\hat{\mathbf{x}}} D_i^\top K_t^\top \end{aligned} \quad (17)$$

$$\begin{aligned} \text{cov}[\mathbf{x}_{t+1}, \mathbf{e}_{t+1}] = & A \text{cov}[\mathbf{x}_t, \mathbf{e}_t] (A - K_t H)^\top \\ & - B L_t \text{cov}[\hat{\mathbf{x}}_t, \mathbf{e}_t] (A - K_t H)^\top \\ & + \Omega^\xi + \sum_i C_i L_t \Sigma_t^{\hat{\mathbf{x}}} L_t^\top C_i^\top \end{aligned} \quad (18)$$

$$\begin{aligned} \text{cov}[\hat{\mathbf{x}}_{t+1}, \mathbf{e}_{t+1}] = & (A - B L_t) \text{cov}[\hat{\mathbf{x}}_t, \mathbf{e}_t] (A - K_t H)^\top \\ & + K_t H \text{var}[\mathbf{e}_t] (A - K_t H)^\top \\ & - K_t \Omega^\omega K_t^\top - \Omega^\eta - \sum_i K_t D_i \Sigma_t^{\hat{\mathbf{x}}} D_i^\top K_t^\top \end{aligned} \quad (19)$$

$$\begin{aligned} \text{var}[\mathbf{e}_{t+1}] = & (A - K_t H) \text{var}[\mathbf{e}_t] (A - K_t H)^\top \\ & + \Omega^\xi + K_t \Omega^\omega K_t^\top + \Omega^\eta \\ & + \sum_i C_i L_t \Sigma_t^{\hat{\mathbf{x}}} L_t^\top C_i^\top + \sum_i K_t D_i \Sigma_t^{\hat{\mathbf{x}}} D_i^\top K_t^\top \end{aligned} \quad (20)$$

**Application to the reaching movement.** The simulated movement task was a single joint reaching movement similar to the study<sup>8</sup>. The movement was replaced with a translational point-to-point reaching movement for simplicity. The movement duration  $t_{end}$  was set to 0.5 s. The starting position was 0 m, while the target position  $p^*$  was 0.2 m.

Parameter	Value
$\Delta t$	0.01 (s)
$m$	1.0 (kg)
$\tau_1$	40.0 (ms)
$\tau_2$	40.0 (ms)
$c$	1

**Table 1.** Parameters of the movement dynamic system.

Parameter	Value
$\omega_p$	0.02
$\omega_v$	0.2
$\omega_f$	1.0
$d$	3

**Table 2.** Parameters of the feedback system.

The matrices of the dynamic system in the translational point-to-point reaching movement are depicted below:

$$A = \begin{bmatrix} 1 & \Delta t & 0 & 0 & 0 \\ 0 & 1 & \Delta t/m & 0 & 0 \\ 0 & 0 & 1 - \Delta t/\tau_2 & \Delta t/\tau_2 & 0 \\ 0 & 0 & 0 & 1 - \Delta t/\tau_1 & 0 \\ 0 & 0 & 0 & 0 & 1 \end{bmatrix}$$

$$B = \begin{bmatrix} 0 \\ 0 \\ 0 \\ \Delta t/\tau_1 \\ 0 \end{bmatrix}$$

$$C_1 = B\sigma_c$$

where  $\Delta t$  is the time step,  $m$  is the point mass, and  $\tau_1$  and  $\tau_2$  are the time constants (Table 1). The state  $\mathbf{x}$  of the system is  $[p(t), \dot{p}(t), f(t), \dot{f}(t), p^*]^\top$ , where  $p$  is the position and  $f$  is the force. The initial state was  $\hat{\mathbf{x}}_1 = [0, 0, 0, 0, p^*]^\top$  and  $\Sigma_1 = 0$ .

The matrices of the feedback system are depicted below:

$$H = \begin{bmatrix} 1 & 0 & 0 & 0 & 0 \\ 0 & 1 & 0 & 0 & 0 \\ 0 & 0 & 1 & 0 & 0 \end{bmatrix}$$

$$D_1 = \sigma_d \begin{bmatrix} \omega_p & 0 & 0 & 0 & 0 \\ 0 & 0 & 0 & 0 & 0 \\ 0 & 0 & 0 & 0 & 0 \end{bmatrix}$$

$$D_2 = \sigma_d \begin{bmatrix} 0 & 0 & 0 & 0 & 0 \\ 0 & \omega_v & 0 & 0 & 0 \\ 0 & 0 & 0 & 0 & 0 \end{bmatrix}$$

$$D_3 = \sigma_d \begin{bmatrix} 0 & 0 & 0 & 0 & 0 \\ 0 & 0 & 0 & 0 & 0 \\ 0 & 0 & \omega_f & 0 & 0 \end{bmatrix}$$

where  $\sigma_d$  is the scaling factor. Table 2 shows the parameters of the feedback system.

The state noise, state-independent observation noise, and internal estimation noise have covariances  $\Omega^\xi = \sigma_\xi^2 \mathbf{I}$ ,  $\Omega^\omega = (\sigma_\omega \text{diag}[\omega_p, \omega_v, \omega_f])^2$ , and  $\Omega^\eta = \sigma_\eta^2 \mathbf{I}$ , respectively. The cost matrices are  $R = r$ ,  $Q_1, \dots, Q_{n-1} = 0$ , and  $Q_n = \mathbf{p}\mathbf{p}^\top + \mathbf{v}\mathbf{v}^\top + \mathbf{f}\mathbf{f}^\top$ , where  $\mathbf{p} = [1, 0, 0, 0, -1]^\top$ ,  $\mathbf{v} = [0, 0.2, 0, 0, 0]^\top$ , and  $\mathbf{f} = [0, 0, 0.02, 0, 0]^\top$ .

The simulated movements were obtained by changing each value of  $\sigma_c$ ,  $\sigma_\xi$ ,  $\sigma_\omega$ ,  $\sigma_d$ ,  $\sigma_\eta$ , and  $r$  in the basic parameter set (Table 3). The optimization was completed when the absolute value of the relative change in the total expected cost became less than the convergence tolerance ( $1.0 \times 10^{-15}$ ).

Parameter	Value
$\sigma_c$	1.5
$\sigma_\xi$	0.0
$\sigma_\omega$	0.0
$\sigma_d$	0.0
$\sigma_\eta$	0.0
$r$	1e-10

**Table 3.** The basic parameter set.

Received: 11 November 2021; Accepted: 26 July 2022

Published online: 03 August 2022

## References

- Morasso, P. Spatial control of arm movements. *Exp. Brain Res.* **42**, 223–227. <https://doi.org/10.1007/BF00236911> (1981).
- Paulignan, Y., MacKenzie, C., Marteniuk, R. & Jeannerod, M. Selective perturbation of visual input during prehension movements. 1. The effects of changing object position. *Exp. Brain Res.* **83**, 502–512. <https://doi.org/10.1007/BF00229827> (1991).
- Osu, R. *et al.* Optimal impedance control for task achievement in the presence of signal-dependent noise. *J. Neurophysiol.* **92**, 1199–1215. <https://doi.org/10.1152/jn.00519.2003> (2004).
- Selen, L. P., Beek, P. J. & van Dieën, J. H. Impedance is modulated to meet accuracy demands during goal-directed arm movements. *Exp. Brain Res.* **172**, 129–138. <https://doi.org/10.1007/s00221-005-0320-7> (2006).
- Liu, D. & Todorov, E. Evidence for the flexible sensorimotor strategies predicted by optimal feedback control. *J. Neurosci.* **27**, 9354–9368. <https://doi.org/10.1523/JNEUROSCI.1110-06.2007> (2007).
- Schmidt, R. A. *et al.* Motor-output variability: A theory for the accuracy of rapid motor acts. *Psychol. Rev.* **86**, 415–451. <https://doi.org/10.1037/0033-295X.86.5.415> (1979).
- Harris, C. M. & Wolpert, D. M. Signal-dependent noise determines motor planning. *Nature* **394**, 780–784. <https://doi.org/10.1038/29528> (1998).
- Todorov, E. Stochastic optimal control and estimation methods adapted to the noise characteristics of the sensorimotor system. *Neural Comput.* **17**, 1084–1108. <https://doi.org/10.1162/0899766053491887> (2005).
- Guigon, E., Baraduc, P. & Desmurget, M. Computational motor control: Feedback and accuracy. *Eur. J. Neurosci.* **27**, 1003–1016. <https://doi.org/10.1111/j.1460-9568.2008.06028.x> (2008).
- van Beers, R. J., Haggard, P. & Wolpert, D. M. The role of execution noise in movement variability. *J. Neurophysiol.* **91**, 1050–1063. <https://doi.org/10.1152/jn.00652.2003> (2004).
- Yeo, S. H., Franklin, D. W. & Wolpert, D. M. When optimal feedback control is not enough: Feedforward strategies are required for optimal control with active sensing. *PLoS Comput. Biol.* **12**, e1005190. <https://doi.org/10.1371/journal.pcbi.1005190> (2016).

## Author contributions

Y.T. conceived and conducted the experiments and analyzed the results.

## Competing interests

The author declares no competing interests.

## Additional information

**Correspondence** and requests for materials should be addressed to Y.T.

**Reprints and permissions information** is available at [www.nature.com/reprints](http://www.nature.com/reprints).

**Publisher's note** Springer Nature remains neutral with regard to jurisdictional claims in published maps and institutional affiliations.



**Open Access** This article is licensed under a Creative Commons Attribution 4.0 International License, which permits use, sharing, adaptation, distribution and reproduction in any medium or format, as long as you give appropriate credit to the original author(s) and the source, provide a link to the Creative Commons licence, and indicate if changes were made. The images or other third party material in this article are included in the article's Creative Commons licence, unless indicated otherwise in a credit line to the material. If material is not included in the article's Creative Commons licence and your intended use is not permitted by statutory regulation or exceeds the permitted use, you will need to obtain permission directly from the copyright holder. To view a copy of this licence, visit <http://creativecommons.org/licenses/by/4.0/>.

© The Author(s) 2022